Numerical Simulation of Atmospheric O_3 at Yosu, Korea and Comparison with Measured Data

Akira Kondo,[(1)] Sang Deug Lee[(2)], Keiichi Yoshimura[(1)], Katsuhito Yamaguchi,[(1)] Akikazu Kaga[(1)]

[(1)] Dep. of Environmental Eng., Osaka University, Yamada-oka 2-1 Suita Osaka 565-0871, Japan

E-mail: kondo@env.eng.osaka-u.ac.jp

[(2)] Dep. of Environmental Eng., Mokpo National University, 61 Dorim-ri, Chungkye-myun, Muan-gun, Chonnam, 534-729, Korea

E-mail: leesang@chungkye.mokpo.ac.kr

Abstract

The atmospheric pollution distribution in the industrial area of Yosu in Korea is calculated using numerical model and the model is validated by comparing the calculations with observed data. The emission of NO_x and SO_x was estimated for 6 sources, and the emission amount of HC was estimated for 9 anthropogenic sources. The calculated wind speed, wind direction and temperature agreed well with the observed data at two observatories, and the calculated concentration of NO, NO_2, O_3 and SO_2 were also reasonable for 5 monitoring stations. The validity of the model is evaluated using 3 indexes of the EPA, and the model is found to be valid and accurate.

Key words: Photochemical oxidant, nitricdioxide, sulfurdioxide, diffusion model, emission

1. Introduction

Although several atmospheric pollutant concentration simulations have been per-

formed for industrial complexes (Scheffe, 1993.; Ohara, 1997), the variability of climate, geography, and pollutant emission in such industrial areas makes it difficult to form a general model for atmospheric pollution. The target region of this research, Yosu, is located in southeast Korea, and Yochon, located south of Yosu, is one of the largest industrial complexes in Korea (Ghim, 1998). The area is seriously affected by atmospheric pollution, and new induction of industry is planned further. The Yosu Regional Environmental Technology Development Center (YETC) was inaugurated in 1999 to address many environmental problems, including atmospheric pollution problems. The organization has been responsible, for example, for establishing automated monitoring systems to regulate emission of atmospheric pollutants from factories.

The Yosu region has a complex shoreline topography and atmospheric pollution is affected by the sea and land breezes. A mountain adjacent to the industrial complex also affects the atmospheric pollution through its effect on local wind. As such local winds dominate the microclimate of the Yosu region, it is difficult to predict the atmospheric pollution using an analysis model like the plume and puff model. Hyun (2001) calculated the wind fields in the Yosu region using a regional atmospheric modeling system (RAMS) and the pollutant diffusion from one imaginary source.

In this paper, we propose an atmospheric pollution model for the Yosu region and compare the calculated results of wind speed and temperature with observed data to verify the validity of the meteorological component of the model. The model is then used to estimate the levels of atmospheric pollutant emission and calculate the atmospheric pollution concentration distribution, and the results are compared with observed data to verify the validity of the diffusion component of the model.

2. Numerical model of atmospheric pollution

The proposed numerical model for atmospheric pollution consists of two compo-

nents; a meteorological model and a diffusion model. The basic equations of the meteorological model consist of momentum equations for wind components u and v, conservative equations for potential temperature and specific humidity, and a hydrostatic equation. The details of this meteorological model are described by Kondo (1996).

2.1. Conservation equation for atmospheric pollution

The conservation equation for atmospheric pollution is expressed as follows using the z* coordinate system.

$$\begin{aligned}\frac{\partial c_{\mathsf{i}}}{\partial t} &= -u\frac{\partial c_{\mathsf{i}}}{\partial x} - v\frac{\partial c_{\mathsf{i}}}{\partial y} - w^*\frac{\partial c_{\mathsf{i}}}{\partial z^*} + \frac{\partial}{\partial x}(K_{\mathsf{H}}^{(\mathsf{c})}\frac{\partial c_{\mathsf{i}}}{\partial x}) + \frac{\partial}{\partial y}(K_{\mathsf{H}}^{(\mathsf{c})}\frac{\partial c_{\mathsf{i}}}{\partial y}) \\ &\quad +(\frac{s}{s-z_{\mathsf{G}}})^2\frac{\partial}{\partial z^*}(K_{\mathsf{V}}^{(\mathsf{c})}\frac{\partial c_{\mathsf{i}}}{\partial z^*}) + R_{\mathsf{i}} + Q_{\mathsf{i}} \qquad (1)\end{aligned}$$

where c is the atmospheric pollutant concentration, u, v and w^* are the wind speed in the directions x, y and z^*, $K_{\mathsf{H}}^{(\mathsf{c})}$ and $K_{\mathsf{V}}^{(\mathsf{c})}$ are the horizontal and vertical turbulent diffusion coefficients, R is the source/sink of chemical reactions, Q is the point source, the subscript i is the chemical species, s is the calculated region height, and z_{G} is the terrain height. The horizontal turbulent diffusion term in Equation (1) was omitted because artificial diffusion by horizontal advection is assumed to be much larger than the horizontal turbulent diffusion. The vertical turbulent diffusion coefficient was determined using the turbulence closure Level 2.5 model (Mellor, 1982). We used the new positive definite advection scheme proposed by Smolarkiewicz (1983) for the advection term, and the central difference for the diffusion term.

2.2. Dry deposition

The deposition resistance consists of a series of aerodynamic resistance, viscous resistance, and surface resistance, and the deposition velocity v_{g} is expressed by

$$v_{\mathsf{g}} = \frac{1}{r_{\mathsf{t}}} = \frac{1}{r_{\mathsf{a}} + r_{\mathsf{b}} + r_{\mathsf{c}}} \qquad (2)$$

where r_t is the total resistance, and r_a, r_b, and r_c are the aerodynamic resistance, the viscous resistance, and the surface resistance. It is difficult to formulize surface resistance as it changes with the state of the ground surface. Here, we classify the land-use into the five categories of urban (artificial surface), forest, rice field, bare soil and water , and gave a resistance value from the literature for each category.

2.3. Chemical reactions

We used the carbon bond chemical mechanism model CBM-IV developed by Gery (1989) as the photochemical reaction model. The CBM-IV mechanism includes 32 species and 81 reactions, involving photochemical, inorganic, and organic reactions.

3. Calculation conditions

3.1. Calculation region

The region of interest, Yosu (local region), has a complex shoreline profile and includes many islands. The flow fields in Yosu are influenced by the synoptic conditions as well as the geographical features. The influence of synoptic flow fields was taken into consideration by incorporating the regional flow fields by the one-way nesting technique. The concentration distribution calculation was carried out only for the local area. The regional scale is defined as a 91 km $\times$ 91 km area (Fig. 1, left) divided into a 91 $\times$ 91 mesh of 1 km $\times$ 1 km cells. The target region (local region) is outlined in Fig. 1, and is a 40 km $\times$40 km area divided into an 80 $\times$ 80 mesh of 500 m $\times$ 500 m cells. The vertical height in both regions is 5000 m, and is divided into 15 layers set at intervals of 8, 8, 8, 8, 48, 129, 210, 290, 371, 452, 532, 613, 694, 774 and 855 m from basal layer. Two meteorological stations (Yosu and Yosu airport) and 5 monitoring stations (Samildong, Joongdong, Teaindong, Jangchondong and Wolledong) exist in the local region. The calculated results were compared with the data observed at these stations. The calculation was carried out for a fine summer

day, conditions that are suitable for high pollutant concentrations.

3.2. Initial and boundary conditions for meteorological prediction model

The initial wind velocity was set at 0 in all calculated regions, the initial potential temperature at sea level was set to 298 K, and the potential temperature above sea level was increased with a constant potential temperature gradient of 0.005 K/m. The initial values of the turbulent variables were determined from the turbulent closure Level 2 model (Mellor, 1982). The surface temperature and specific humidity were determined by solving the ground surface heat budget equation proposed by Deardorff (1978). The bottom boundary values of potential temperature, specific humidity and wind velocity were determined from the similarity theory of Monin-Obukhov. The lateral boundary values of the larger region were determined assuming a gradient of 0. The lateral boundary values in the local region were determined by the one-way nesting technique (Ikawa, 1991).

3.3. Initial and boundary conditions of atmospheric pollutant concentration prediction model

The initial values of the main species are shown in Table 1. It was assumed that the upper boundary values did not change during the calculation and the lateral boundary values were determined assuming a gradient of 0. The bottom boundary values were specified by the flux F in the following equation

$$F = -v_{\mathsf{g}} \cdot c + Q_{\mathsf{sf}} \tag{3}$$

where Q_{sf} is the emission flux from the ground surface and v_{g} is the deposition velocity.

3.4. Calculation procedure

Performing the flow and concentration calculations simultaneously requires lengthy

calculation times. Therefore, the flow calculation was performed in advance and the data required for the concentration calculation was saved to hard disk.

4. Emissions of SO_x, NO_x and HC

The emission levels of SO_x, NO_x and HC in the local region were estimated using the proposed model. The sources of SO_x and NO_x emission were classified into 6 categories; Airplane, Factory, Household, Railroad, Vehicle, and Ship. The estimated emissions of SO_x and NO_x are shown in Table 2. The emissions of SO_x and NO_x from factories were 69054 t/yr and 31445 t/yr, respectively, representing about 83.9% and 84.2% of the total emissions. The next most significant source of SO_x emission was ships, and that of NO_x emission was vehicles. The emission distribution for NO_x is shown in Fig. 2. Power plants and steel plants located along the shoreline in Kwang-Yang Bay are responsible for high emission level, as is the main road connecting Yosu and Sunchon. The anthropogenic sources of HC emission were classified into 10 categories; Airplane, Factory, Household, Railroad, Vehicle, Ship, Gasoline Vapor, Painting, Construction Painting, and Cleaning. The estimated emissions of HC are shown in Table 3. Factories, vehicles, and construction painting made up about 89.7% of the total anthropogenic HC emission. Forest and rice fields emit HC in the form of mono-terpene, α-pinene and Isoprene. These natural emissions were estimated from the emission factor to be $3231\mu g/(m^2\ h)$ for forests and $510\mu g/(m^2\ h)$ for rice fields (Kondo, 1999).

4.1. Effective stack height

The emissions from factories and ships were treated as point sources (Q in Equation (1)) and the emissions from other sources were treated as area sources. The effective stack height was calculated using the European Oil Company Organization for Environment, Health and Safety (CONCAWE) formula for windy conditions (wind

speed ¿1.0 m/s) and from Briggs's formula for calm conditions (wind speed ¡1.0 m/s). As no statistical data is available for stack height, the amount of exhaust gas, or the temperature of exhaust gas for ships in Yosu, this data was assumed to be the same as that for the passage of ships through Akashi Strait in Japan (Kondo, 1999).

4.2. Diurnal variations in emission quantities

The diurnal variations in emissions from vehicles, factories and ships were determined from statistical data for Japan (Fig. 3). The emissions from other sources were assumed to be constant throughout the day.

5. Comparison of calculated results and observed data

5.1. Comparison of wind vectors and temperature

The horizontal distribution (12 m height) of the calculated regional flow field is shown in Fig. 4 for intervals of 4 h. Similarly, the horizontal distribution (12 m height) of the calculated flow field in the local region are shown in Fig. 5 for intervals of 4 h. From Fig. 4, the sea breeze can be seen to develop strongly during the day, and the land breeze is weak at night. At night, the mountain wind follows complex geographical features. Figure 5 also shows the strong daytime sea breeze. However, at night, the wind direction varies significantly due to the complex topography of the shoreline.

The diurnal variations in the calculated and observed wind vectors at Yosu and Yosu airport are shown in Fig. 6. The observed wind direction represents the prevailing wind direction each hour in August 2000, except for cloudy days, and the wind speed is the average for August 2000 except for cloudy days. These values were assumed because the calculation was carried out for a typical fine summer day. From the observed wind vectors, the prevailing sea breeze comes from the SES

during the day, and the land breeze comes from the NNW at night. The wind speed in Yosu is much stronger than that at Yosu airport. The calculated wind vectors in Yosu are reasonably consistent with the observed results except for the wind speed at night. The calculated wind vectors at Yosu airport differed from the observed results in terms of the conversion time to sea breeze from land breeze and the wind speed. The diurnal variations in the calculated and observed temperature at Yosu and Yosu airport are shown in Fig. 7. The observed temperature represents the average temperature in August 2000 except for cloudy days. The calculated daytime temperature at Yosu airport is lower than the observed temperature, whereas the calculated temperature in Yosu is correct. This inconsistency for Yosu airport is attributed to the fact that the airport does not fit correctly into any of the land-use categories in the numerical model. However, the general characteristics of the typical climate for August in the Yosu region appeared to be well reproduced by the numerical model.

5.2. Comparison of atmospheric pollutant concentrations

The diurnal variations in the calculated and the observed NO, NO_2, O_3, and SO_2 concentrations are shown in Figs. 8 to 11. The observed concentrations represent the average concentrations for August 2000 excluding cloudy days. The calculated NO and NO_2 concentrations underestimate the observed concentrations at all monitoring stations. However, the calculated O_3 concentration agreed remarkably well with the observed concentration at all monitoring stations. The inaccurate NO and NO_2 estimation is thought to be due to an underestimation of the emission of NOx, however the agreement of the O_3 concentration suggests that the emission levels were estimated reasonably, even for NO_x. It is considered necessary to measure concentration at many locations in order to solve this problem The calculated SO_2 concentration also agreed remarkably well with the observed concentration. How-

ever, the calculated SO_2 concentration included a few peaks at monitoring stations located immediately leeward of factories with high pollutant emission levels. The area of high pollutant concentration was larger during the day than at night because of the relatively high wind speed. The area of high concentration rotated clockwise with the wind direction. It is thought that the observed concentration becomes evenly distributed due to the large variation in wind direction. These results indicate that the model used in this simulation is capable of predicting the distribution of atmospheric pollutant concentration with reasonable accuracy.

5.3. Accuracy of calculated O_3 concentration

The accuracy of the calculated O_3 concentration was evaluated using the Environmental Protection Agency (EPA) indexes (EPA, USA, 1991) of normalized gross error (NGE), normalized gross bias (NGB) and unpaired highest-prediction accuracy (HPA), defined by the following equations.

$$NGE = \frac{1}{n \times H} \sum_{i=1}^{n} \sum_{j=1}^{H} \frac{|C_{obs} - C_{cal}|}{C_{obs}} \leq 0.30 \sim 0.35 \tag{4}$$

$$NGB = \frac{1}{n \times H} \sum_{i=1}^{n} \sum_{j=1}^{H} \frac{C_{obs} - C_{cal}}{C_{obs}} \leq (0.05 \sim 0.15) \tag{5}$$

$$HPA = \frac{C_{obs,max} - C_{cal,max}}{C_{obs,max}} \leq (0.15 \sim 0.20) \tag{6}$$

where C_{obs} and C_{cal} are the observed and calculated values, n is the number of observation stations and H is the number of measurements. $C_{obs,max}$ and $C_{cal,max}$ are the highest observed value and the highest calculated value among all observatories and all measurements. NGE and NGB were estimated for observed data exceeded 20 ppb, and the values obtained were 0.33 and 0.02, respectively. The HPA value was -0.18. These values are within the target values of the EPA (the last values in Equations (4) to (6)). This indicates that the calculated O_3 concentration in

the Yosu region for August was accurately reproduced by the proposed atmospheric pollutant prediction model.

6. Conclusion

The distribution of atmospheric pollution in the industrial area of Yosu in Korea was calculated using a newly defined model. The calculation was carried out for a fine summer day, which is likely to produce high pollutant concentrations. The emissions of NO_x and SO_x were estimated for 6 different sources, and factory emissions were confirmed to form the majority of these emissions. The emission of HC was estimated for 9 sources, and it was found that factories, vehicles and construction painting comprised about 90% of all anthropogenic HC emissions. The calculated wind speed, wind direction and temperature were in good agreement with the observed data in two observatories, and the calculated concentration of NO, NO_2, O_3 and SO_2 were also reasonable for 5 monitoring stations. Inconsistencies were identified and areas of improvement were suggested. The calculated pollutant concentration was verified to agree with the observed results based on 3 indexes set out by the EPA. The numerical model used here has been demonstrated to be capable of reproducing atmospheric pollution distributions for the Yosu region, and may be useful for developing countermeasures to atmospheric pollution in that area.

References

Ikawa, M., Saito, K. , 1991, Description of Nonhydrostatic Model Developed at the Forecast Research Department Of the MRI, Technical Reports of the MRI, 28

Deardorff, J. W. , 1978, Efficient prediction of ground surface temperature and moisture with inclusion of a layer of vegetation, J. Geophys. Res., 83, 1889-1903

Gery, M.W., Whitten, G.Z., Killus, J.P., Dodge, M.C. , 1989, A Photochemical Kinetics Mechanism for Urban and Regional Scale Computer Modeling, J. Geophys. Res., 94, 12925-12956

Ghim, Y.S, Song, C.H., Shim, S.G., Kim, Y.P., Moon, K.C. , 1998, Comparative study of volatile organic compound concentrations in the Yochon industrial estate during and fall (in Korea), Journal of Korea Air Pollution Research Association, 14, 153-160

Kondo, A., Yamaguchi, K., Ahn, H.K. , 1996, Simulation of Climatic Effects by construction of Reclaimed Island in Pusan, Korea, Atmospheric Environment, 30, 2437-2448

Kondo,A., Yamaguchi,K., Nishikawa,E. , 1999, Influence of Ship Emission on Atmospheric Pollutant Concentration around Osaka Bay Area, Japan., WIT press, Air Pollution VII, 415-424

Mellor, G.L., Yamada, T. , 1982, Development of a Turbulence Closure Model for Geophysical Fluid Problems., Review Geophys. and Space Phys. ,20, 851-875

Oh, H.S., Ghim Y.S. , 2001, Numerical study of atmospheric dispersion of a substance released from an industrial complex in the southern coast of Korea, Atmospheric Environment, 35, 3103-3111

Ohara, T., Wakamatsu, S., Uno, I., et.al , 1997, Development and Validation of Numerical Model for Photochemical Oxidants., J. of Jpn Soc. Atmospheric Environment, 32, 6-28 (in Japanease)

Scheffe, Y.S, Morris, R.E. , 1993, A review of the development and application of the urban airshed model, Atmospheric Environment, 27B, 23-39

Smolarkiewicz, P.K. , 1983, A Simple Positive Definite Advection Scheme with Small Implicit Diffusion, Mon. Wea. Rev., 111, 479-486

U.S. Environmental Protection Agency , 1991, Guideline for regulatory application of the Urban Airshed Model, EPA-450/4-91-013

Table 1: Initial concentrations [ppb].

Species	0m $\sim$ 209m	209m $\sim$
NO	15	2
NO_2	15	2
O_3	20	20
SO_2	10	10

Table 2: Emission amount of SO_x and NO_x.

Source	SO_x t/yr	Ratio %	NO_x t/yr	Ratio %
Airplane	0	0	50	0.1
Factory	69,054	83.9	31,445	84.2
Household	2,693	3.3	801	2.1
Railroad	42	0.1	274	0.7
Vehicle (Main road)	226	0.3	3,475	9.4
Vehicle (Minor road)	30	0.0	467	1.3
Ship	10,237	12.4	826	2.2
Total	82,282	100.0	37,338	100.0

Table 3: Emission amount of anthropogenic HC.

Source	Emission t/yr	Ratio %
Airplane	121	2.4
Factory	2,648	52.5
Household	22	0.4
Railroad	68	1.3
Vehicle(Main road)	951	18.9
Vehicle(Minor road)	128	2.5
Ship	94	1.9
Gasoline Vapor	15	0.0
Painting	2	0.0
Construction Painting	766	15.3
Cleaning	238	4.8
Total	5,053	100.0

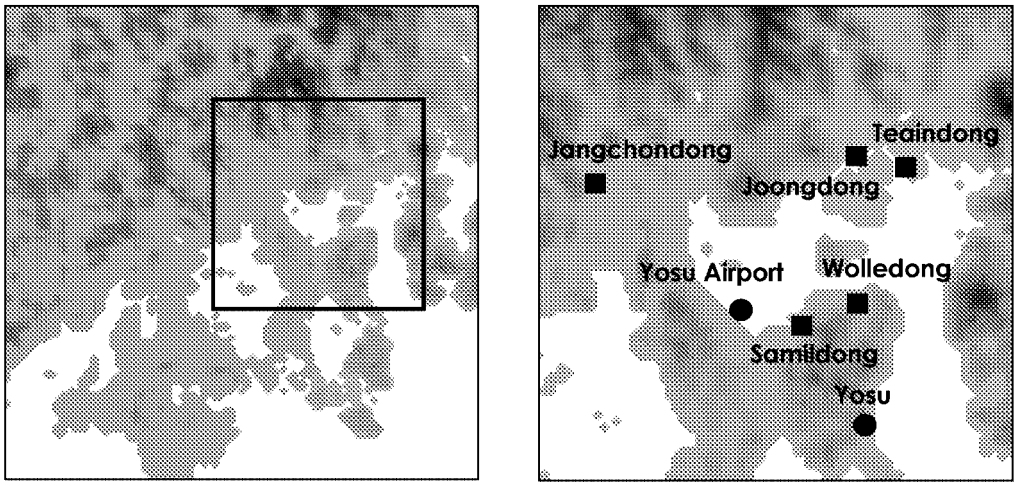

Figure 1. Target region. (Left) Large region with outline of local region. (Right) Local region. Circles, meteorological monitoring stations; squares, air pollution monitoring stations.

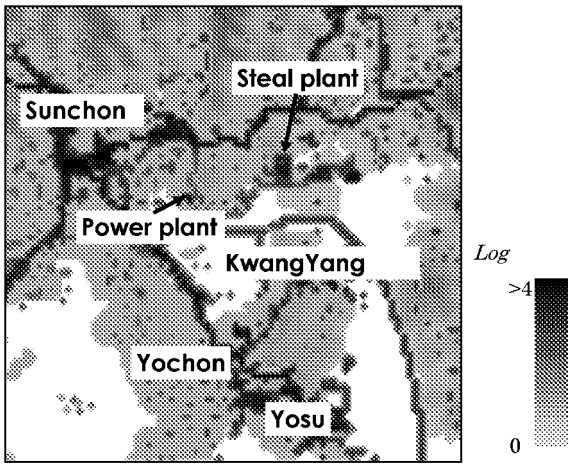

Figure 2. Emission distribution for NO_x

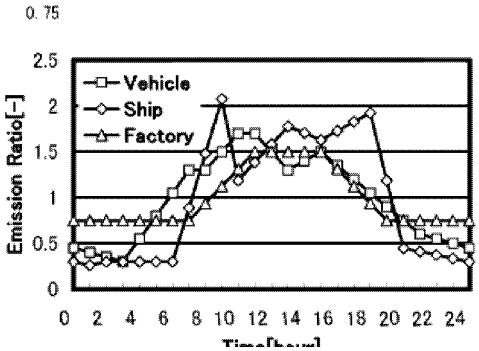

Figure 3. Diurnal variation in emissions for Ship, Factory and Vehicle

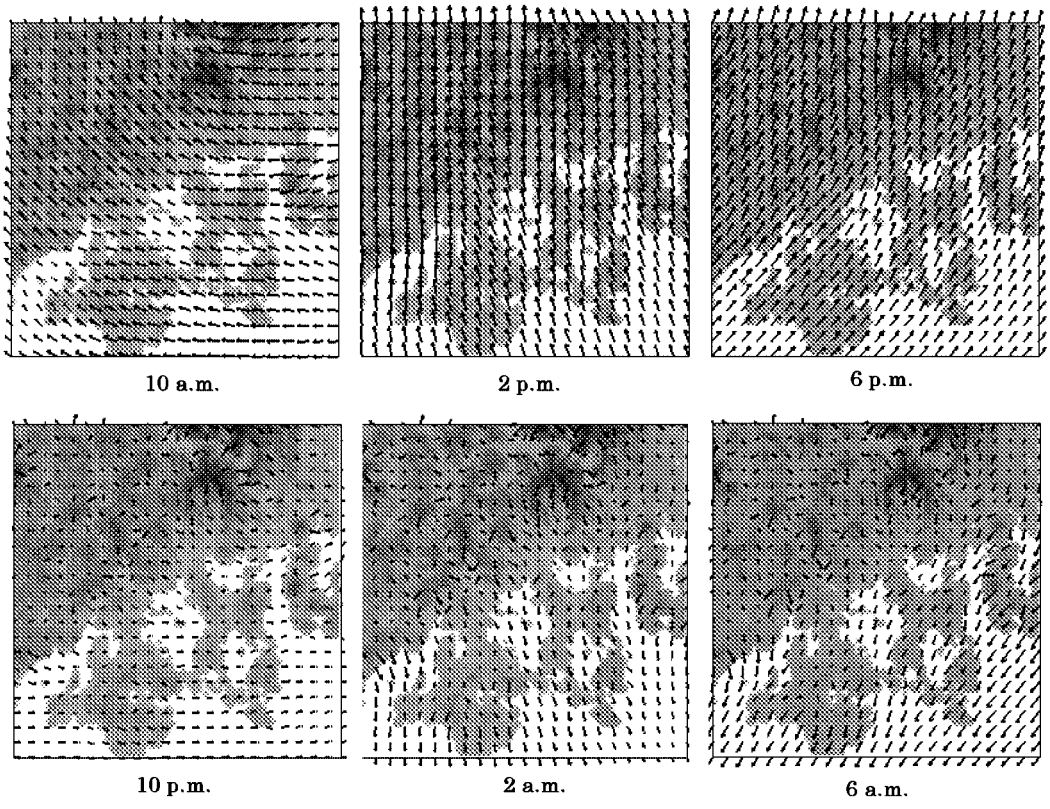

Figure 4. Distribution of wind vectors in large region at 4 h intervals (12 m height)

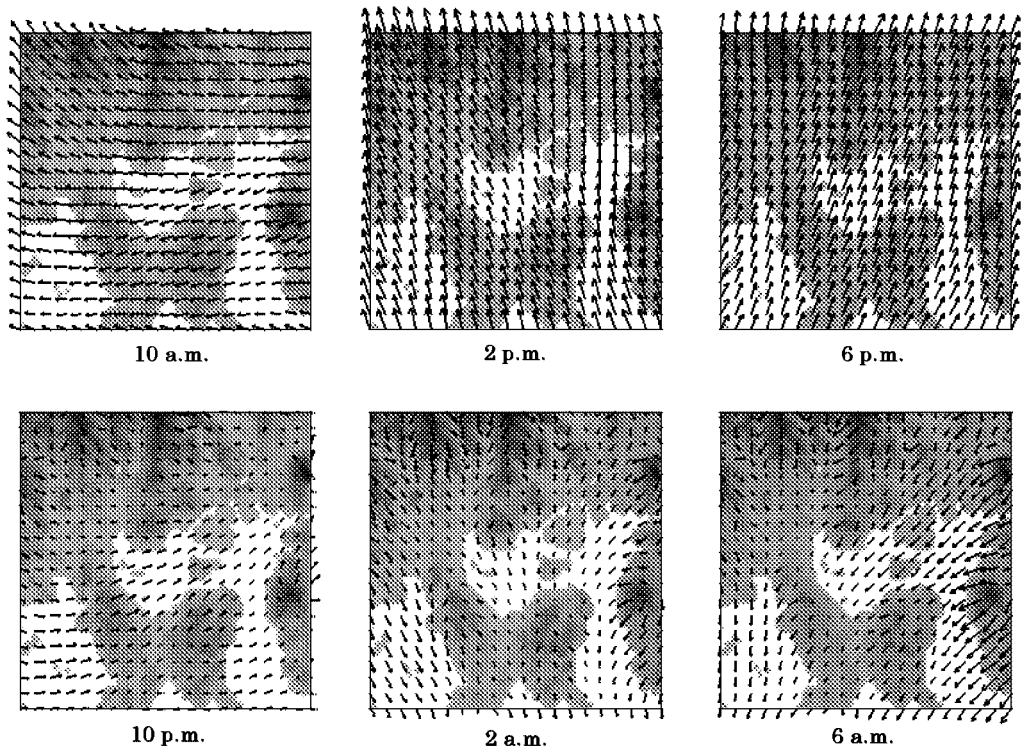

Figure 5. Distribution of wind vectors in small region at 4 h intervals (12 m height)

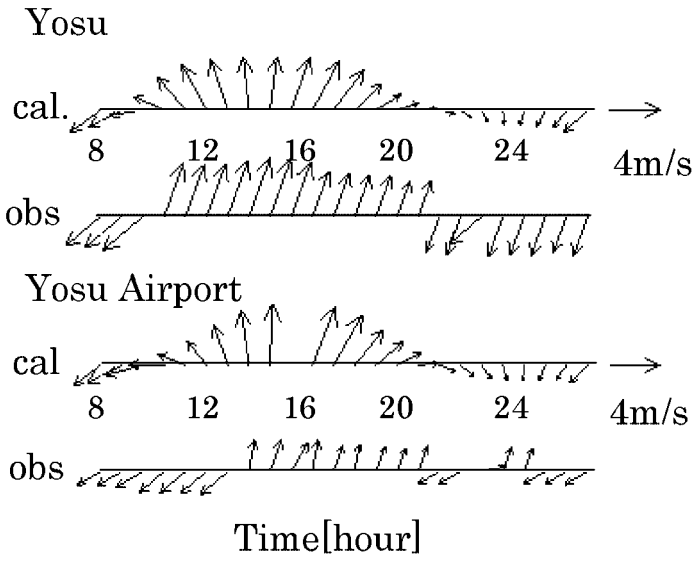

Figure 6. Diurnal variation in wind vectors at Yosu and Yosu airport. Upper, calculated; lower, observed.

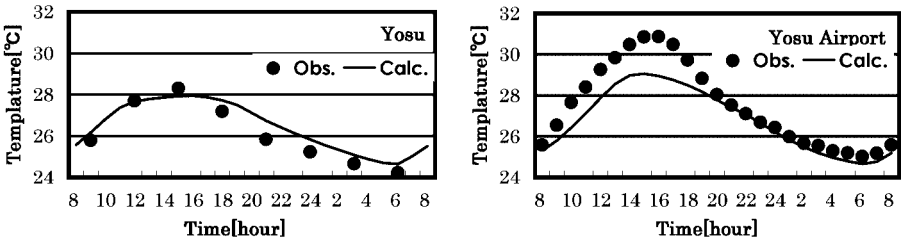

Figure 7. Diurnal variation in temperature at Yosu and Yosu airport

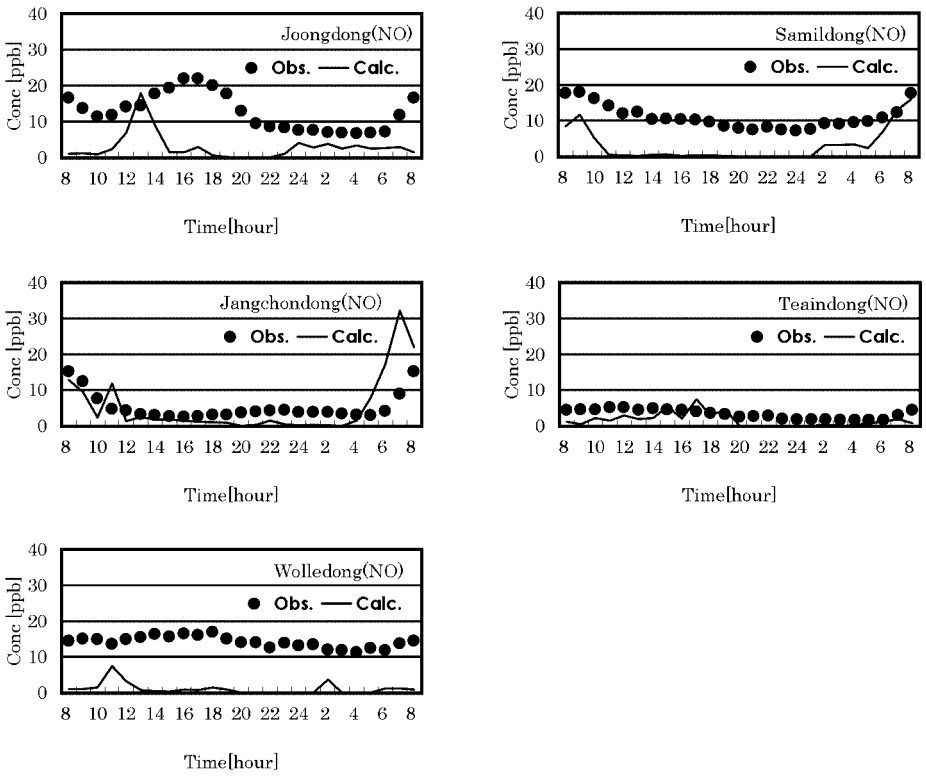

Figure 8. Diurnal variation in NO concentration at 5 monitoring stations

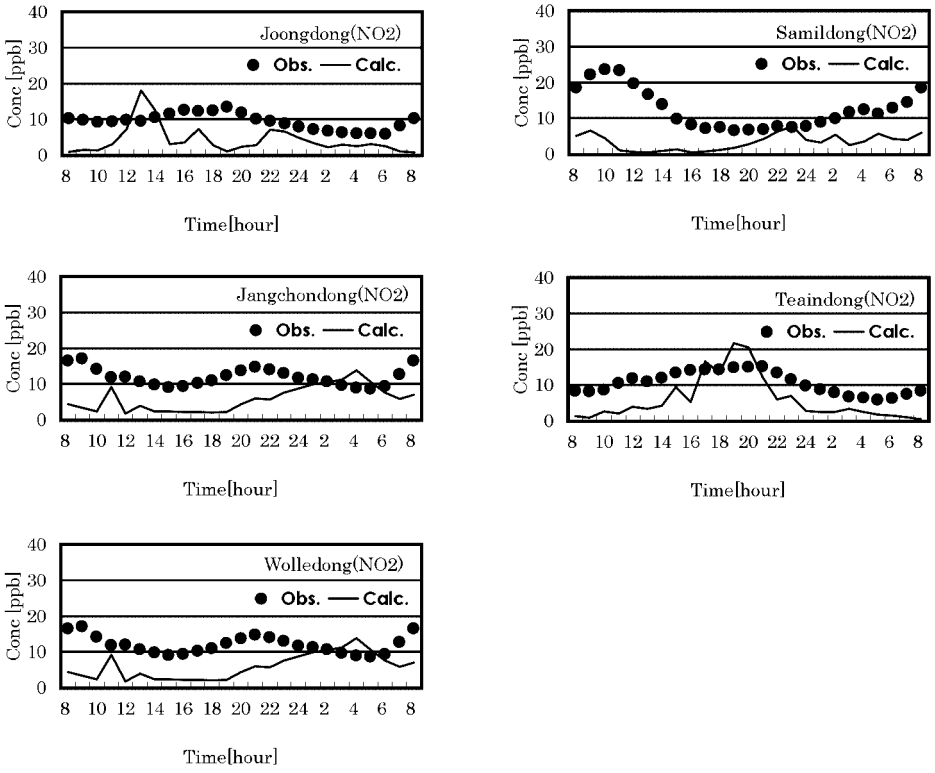

Figure 9. Diurnal variation in NO_2 concentration at 5 monitoring stations

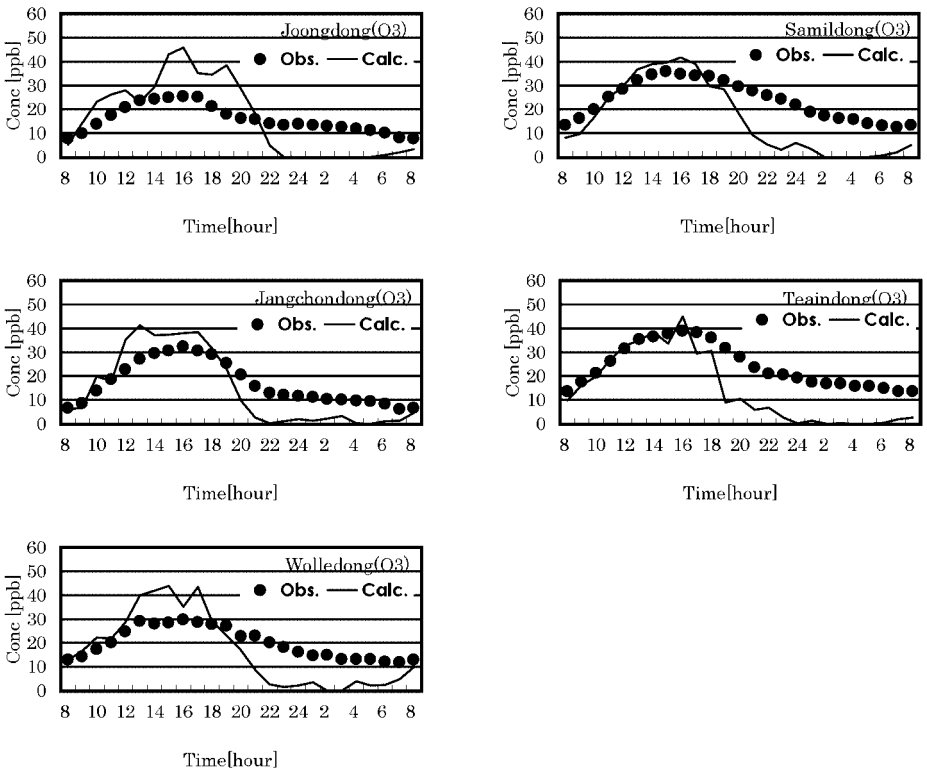

Figure 10. Diurnal variation in O_3 concentration at 5 monitoring stations

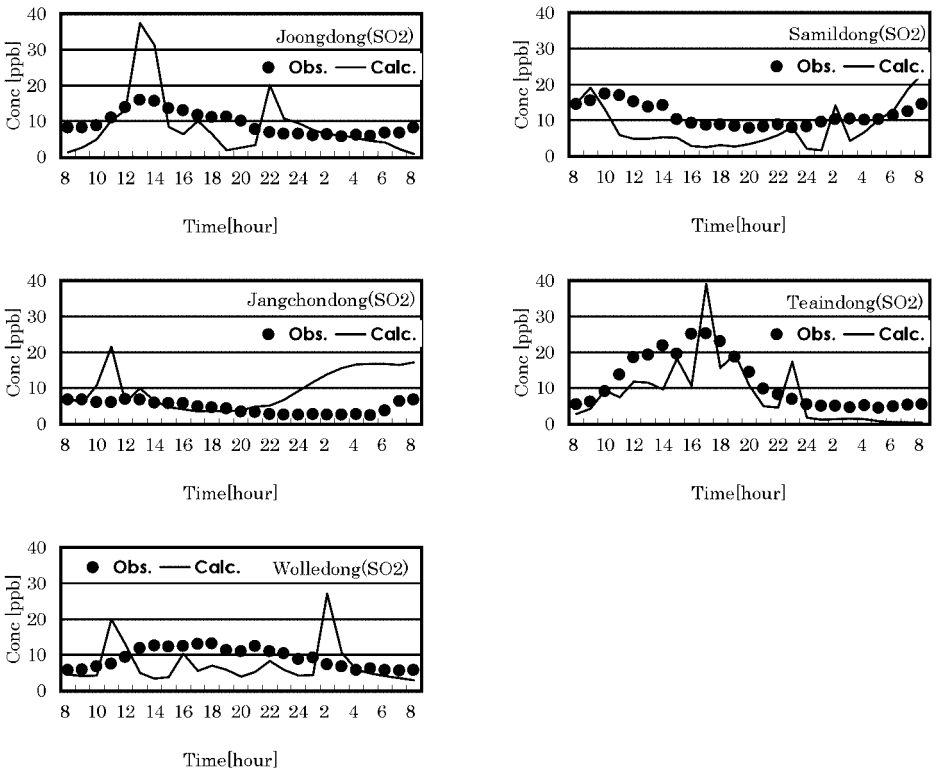

Figure 11. Diurnal variation in SO2 concentration at 5 monitoring stations